Characterising dust in JET with the new ITER-like wall

2015 Plasma Phys. Control. Fusion 57 014037

(http://iopscience.iop.org/0741-3335/57/1/014037)

OPEN ACCESS
IOP Publishing
Plasma Physics and Controlled Fusion
Plasma Phys. Control. Fusion **57** (2015) 014037 (11pp)
doi:10.1088/0741-3335/57/1/014037

Characterising dust in JET with the new ITER-like wall

J C Flanagan[1,10,11], M Sertoli[2], M Bacharis[3], G F Matthews[1], P C de Vries[4], A Widdowson[1], I H Coffey[5], G Arnoux[1], B Sieglin[2], S Brezinsek[6], J W Coenen[6], S Marsen[2], T Craciunescu[7], A Murari[8], D Harting[1], A Cackett[1], E Hodille[9] and JET-EFDA Contributors[12]

JET-EFDA, Culham Science Centre, Abingdon, OX14 3DB, UK
[1] CCFE, Culham Science Centre, Abingdon, Oxon, OX14 3DB, UK
[2] Max-Planck-Institut für Plasmaphysik, EURATOM Association, 85748 Garching, Germany
[3] Imperial College of Science and Technology, London, SW7 2AZ, UK
[4] ITER Organization, Route de Vinon-sur-Verdon, CS 90 046, 13067 St. Paul Lez Durance Cedex, France
[5] Queen's University, Belfast, BT7 1NN, UK
[6] Forschungszentrum Juelich GmbH, EURATOM Association, 52425 Juelich, Germany
[7] EURATOM-MEdC Assoc., Inst. for Laser, Plasma and Radiation Physics, Romania
[8] Consorzio RFX-Associazione EURATOM ENEA per la Fusione, I-35127 Padova, Italy
[9] IRFM, CEA Cadarache, 13108 Saint Paul Lez Durance, France

E-mail: joanne.flanagan@ccfe.ac.uk

Received 24 June 2014, revised 12 September 2014
Accepted for publication 25 October 2014
Published 28 November 2014

Abstract

Recent studies dedicated to the characterisation of in-vessel dust in JET with the new ITER-like wall (ILW) show that dust levels are orders of magnitude lower compared with the latter stages of the carbon-wall (CW) period and are decreasing with operational time. Less than 1 g of dust was recovered in a recent inspection, compared with more than 200 g of material recovered at the end of the JET-CW life. Recent inspection of the ILW shows low rates of re-deposition with only small areas of damage of a type likely to create particulate matter. Quantifiers from laser scattering techniques also indicate an order of magnitude reduction in dust relative to the JET-CW and show that the amount of dust mobilized after a disruption is proportional to the dynamic vessel forces. It is not possible to infer what fraction of dust (if any) might be created by disruptions. However, disruption mitigation is found to reduce the amount of dust seen after moderate disruptions by a factor of 4. Analysis of the transient impurity events (TIEs) associated with dust show that tungsten dominates. A significant contribution to TIEs is also seen from iron, nickel and chromium (probably from steel and Inconel components). The incidence of severe negative effects on operations from TIEs is found to be relatively rare, with <1% of ILW disruptions linked to TIEs. The evolution of the TIE rate closely follows changes in the laser scattering dust quantifiers; both trend downwards in time but peak during periods of higher disruption rate (thought to be primarily driven by the mobilization of existing dust).

Keywords: ITER-like wall (ILW), dust, transient impurity events, JET, tokamak, UFO

(Some figures may appear in colour only in the online journal)

1. Introduction

1.1. Dust

In this paper we focus on results from studies of dust in JET with the new ITER-like wall. However, in-vessel dust in magnetic fusion devices has been the topic of a large number of

[10] Invited speaker.
[11] Author to whom any correspondence should be addressed.
[12] See the appendix of Romanelli *et al* 2012 *Proc. of the 24th IAEA Fusion Energy Conf.* (*San Diego, USA*).

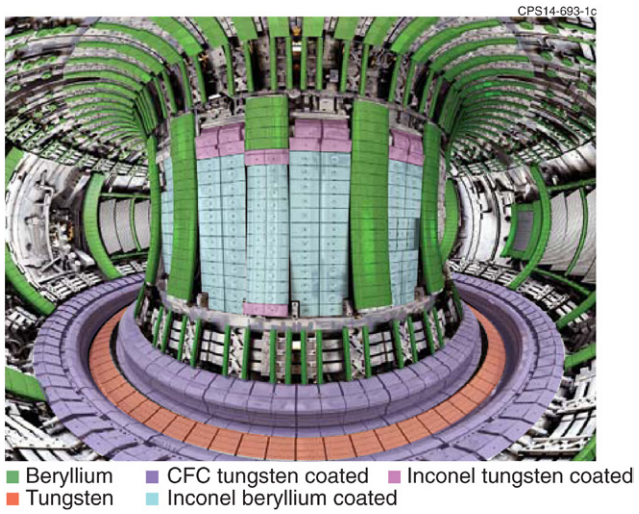

Figure 1. Photograph of the JET ITER-Like Wall (ILW). Coloured shading indicates material composition.

studies and for a review of this area in general we direct the reader to (Krasheninnikov 2011, Ratynskaia 2011). In-vessel dust is loosely defined as particulate matter up to ~1 mm in size and is produced via plasma interaction with plasma-facing components and also via physical trauma during in-vessel maintenance / enhancement works (Rosanvallon 2009). As such, dust primarily consists of the materials that makeup the in-vessel environment. In JET's current ITER-like wall (ILW) configuration, the plasma facing components (PFCs) principally consist of beryllium (Be) and tungsten (W), with bulk Be tiles and W-coated carbon fibre composite (CFC) tiles and bulk W tiles used in the higher heat flux areas. Nickel, iron and chromium are also present via steel and Inconel components (i.e. supporting structures). Figure 1 shows JET's ITER-like wall, with the different materials shaded according to their composition. For a more detailed description we refer the reader to (Matthews 2011) and references therein.

In-vessel dust has important implications for plasma operations and safety in the tokamak environment, particularly in future long-pulse devices such as ITER (Rosanvallon 2009). Transient impurity events (TIEs), thought to be caused by small particles or dust contaminating the core plasma, are typified by a sharp increase in radiated power (Coenen 2013, Sertoli 2014). TIEs can harm plasma performance and have the potential to lead to instability events and can abruptly terminate the plasma discharge (Ekedahl 2009, de Vries 2014, Sertoli 2014). Large volumes of dust also present safety issues in terms of tritium retention and the potential for volatile interaction in the event of air or water ingress into a hot vessel (Bell 2002, Roth 2009). The current ITER strategy in response to these concerns is to measure and minimise the dust inventory (Rosanvallon 2009). Building an understanding of dust characteristics and their impact on plasma operations within current devices is thus essential to this goal.

1.2. Disruptions

During a disruption, the growth of plasma instabilities impairs confinement and causes a rapid and large loss of thermal energy (referred to as the thermal quench). This typically leads to the loss of plasma current (the current quench) and is often accompanied by a loss of vertical stability, called a vertical displacement event (de Vries 2014). The fast release of magnetic energy often results in large forces transferred to the mechanical structure of the vessel, causing it to shake. Disruption forces of up to 4 MN have been recorded at JET (in both CW and ILW operational periods), with disruption forces of >1 MN commonplace. Measurement of the vessel forces on JET are made by strain gauges placed on each of the vessel's 32 support legs (Marchese 1996, Lescure 2009). During the thermal quench, high heat-loads can also be transferred onto the PFCs. The relatively delicate nature of JET's ILW (Be melts at ~1300 °C) has necessitated the development of disruption mitigation methods based on a massive gas injection (MGI), delivered just prior to plasma termination (Lehnen 2010). Mitigation by MGI has been shown to significantly decrease the sideways forces during vertical displacement events. The heat loads during the thermal quench can also be reduced by the enhancement in energy radiated from the plasma that is seen with MGI (Lehnen 2010, de Vries 2014). Timing parameters relating to JET disruptions are defined here as: the disruption time t_d, which is equal to the onset of the thermal quench; and the time of maximum vessel displacement t_m, which marks the point at which one may expect to see disruption related mobilization occurring. Both of these times are given relative to the start of the plasma at $t = 0$ s.

1.3. Overview

In this work, we aim to provide answers to some key questions on the topic of in-vessel dust for JET's new ILW; e.g. how much dust is there and what is it made from? How does this compare to previous phases of operations with the CFC wall? What are the sources of dust and what impact does the current dust inventory have on plasma operations? Are there particular events that we should strive to avoid in terms of dust production / mobilization? How is the amount of dust changing with time? At what point does the dust inventory become a real problem and is active mitigation necessary? What does this mean for future devices, such as ITER? Answering these questions is only possible by studying the properties of the in-vessel dust at frequent intervals, including dust related events occurring during plasma operations. Consequently, remote methods of dust and TIE analysis are essential and are considered in addition to the assessment of information and material gathered during in-vessel studies (for which manned access is, briefly, necessary). The methods considered here are:

(a) Images of events during operations from JET's numerous camera-based monitoring systems
(b) VUV spectroscopy of TIEs during plasma discharges
(c) Analysis of photo surveys and dust collection performed during a recent in-vessel inspection
(d) Laser scattering from dust mobilized by disruptions

The experimental methods of observing dust and related events are described in detail in section 2, together with

Figure 2. Frames from images from JET's COHU colour CCD camera (KL1) from octant 4 for JET pulse 80706. The plasma is terminated by a disruption with $t_d = 14.17$ s and $t_m = 14.25$ s. Induced vessel forces are recorded as 2.52 MN. A cloud of debris is seen at $t = 14.24$ s and in subsequent frames.

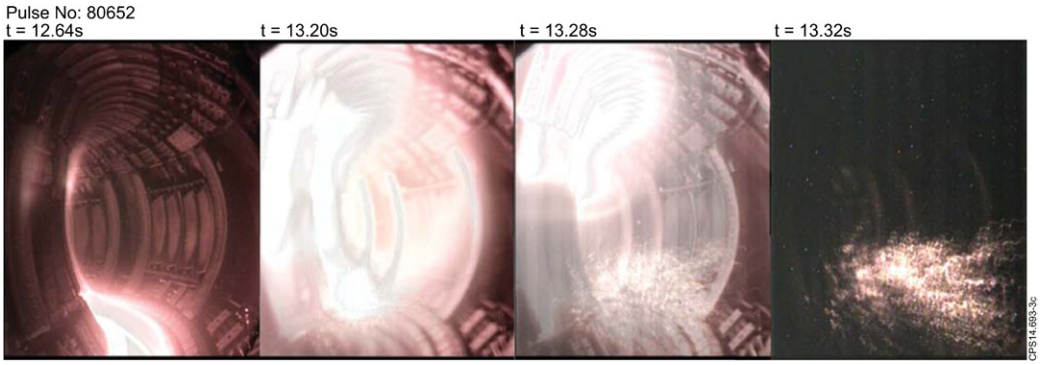

Figure 3. Images from JET's COHU colour CCD camera (KL1) from octant 4 for JET pulse 80652. The plasma is terminated by a disruption with $t_d = 13.14$ s and $t_m = 13.18$ s. Induced vessel forces are recorded as 0.43 MN. A cloud of debris is seen at $t = 13.20$ s and in subsequent frames. Note that the images in frames after $t = t_d$ show distortion due to camera shaking.

results for JET's recent operational period with the ILW. Where possible, comparisons to results from JET's carbon-wall (CW) period are made. Theoretical modelling of the interaction of plasma and dust is another valuable source of information; one that has the potential to bridge the gaps in knowledge obtained through remote observations and can also give a deeper understanding of the physical mechanisms responsible for impurity radiation events. Results from numerical modelling work on the dust-plasma interaction in JET presented in (Sertoli 2014) are highlighted for comparison within section 2 where relevant. Discussion and conclusions are presented in section 3.

2. Experimental methods and results

A summary of results from four methods of monitoring in-vessel dust are presented here; a) camera imaging, b) VUV spectroscopy, c) in-vessel inspection (including physical dust collection) and d) laser scattering after disruptions.

2.1. Camera systems

JET houses numerous visible and infrared camera systems that make real-time observations of the plasma chamber; to monitor the plasma and the plasma facing components. A systematic analysis of this type of data over the many thousands of JET pulses is a formidable task, and not one that we consider here. Instead, we look to this source of information for a few events of particular interest; to assist in the understanding and the benchmarking of data from other sources and to highlight events for further study. However, we note that the automatic analysis of defects (such as particulate matter) on the horizontal surfaces of JET's divertor tiles has been demonstrated (Craciunescu 2014a 2014b).

JET's camera systems are often particularly illuminating in the case of disruptions and often capture particles shaken loose by the vessel displacement, as seen in figures 2 and 3, which show sequential video frames from the KL1 camera for JET pulse 80706 and 80652 respectively. In both instances a cloud of glowing debris is visible just after the disruption. When sequential frames are viewed, the dust seen in figure 2 appears to be rotating, centred around the middle of the vessel, while the dust in figure 3 moves from the vessel centre to the outer divertor region and does not rise above the mid-plane of the vessel. The fact that dust does not uniformly fill the vessel in these events is important when interpreting data from diagnostic systems with narrow lines of sight. Disruptions can also lead to high heat-loads onto the PFC, which are closely monitored by JET's infrared protection camera systems (Arnoux 2010). In extreme heat-load events, melting of parts of the Beryllium PFCs as the plasma terminates has been observed. In JET pulse 85943, an experiment studying runaway electrons disrupted after the runaways doubled past the intended

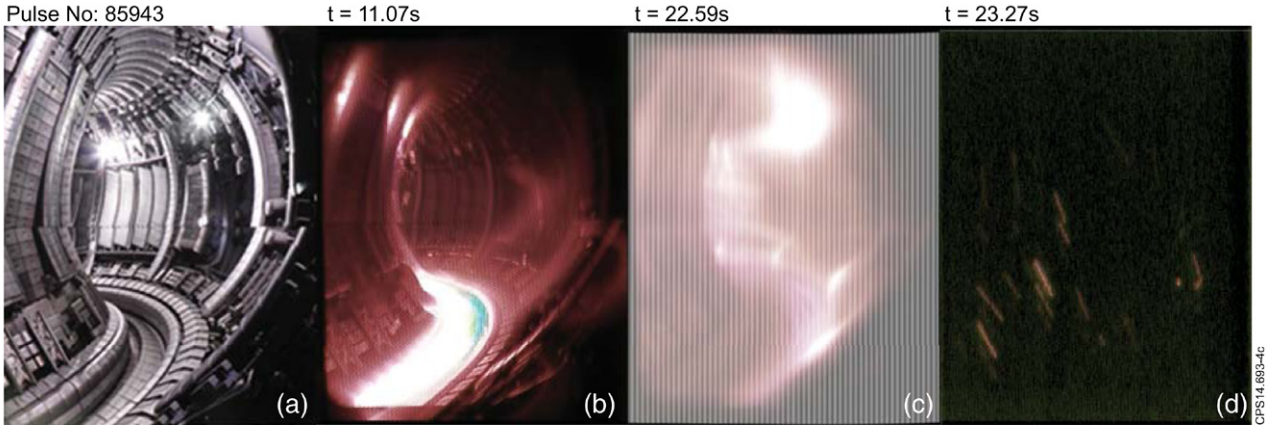

Figure 4. (*a*) View from octant 5, as seen by the high resolution DSLR camera (KL14) with the internal vessel lights on. (*b*)–(*d*) Frames from KL14 for JET pulse 85943. The plasma is terminated by a disruption with $t_d = 22.53$ s and $t_m = 22.59$ s. Induced vessel forces are recorded as 0.90 MN. (*d*) Sometime after the initial disruption (at $t = 23.10$ s onwards), particles can be seen falling from an upper part of the vessel into the divertor region.

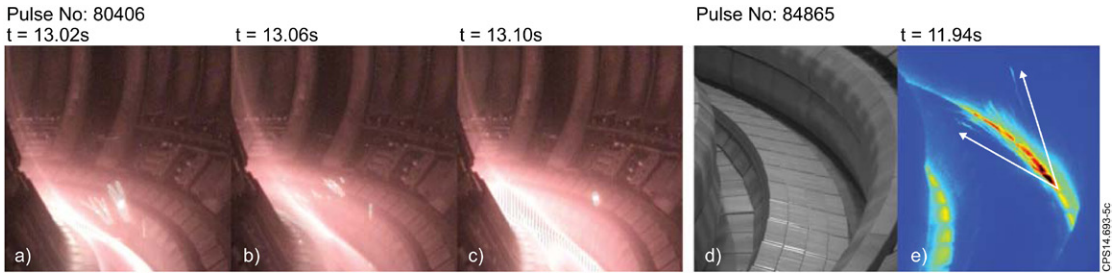

Figure 5. Images showing influx of particulate matter into the JET plasma. (*a*)–(*c*) JET's COHU colour CCD camera (KL1) from octant 4 for JET pulse 80406, (*d*) Divertor view from octant 1 as seen by the AVT-PIKE camera (KL11) (Huber 2012), with the internal vessel lights on (*e*) frame from KL11 for JET pulse 84865.

number. The resultant high heat-load on the upper dump plates caused partial melting. Droplets of beryllium were seen to rain down into the divertor region, as shown by the video frames from KL14, a high resolution DSLR camera, in figure 4. This is JET's most sensitive visible camera; the slight distortion in the image is due to the complex optics of this system, which includes in-vessel mirrors (Clever 2013).

The influx of particles into the JET plasma is also sometimes captured by camera systems; see examples in figure 5. JET pulse 80406 disrupted soon after the particle influx shown in figures 5(*a*)–(*c*), while the particles seen entering the plasma in JET pulse 84645 (figure 5(*e*)) resulted in a large TIE and significantly lowered the pedestal temperature. In both of these cases, VUV analysis identified tungsten as the responsible impurity (see section 2.2 for more details). Images of this type allow the particle trajectory and velocity at input to be approximated; parameters which will serve as useful inputs to any modelling effort (as described in section 2.3).

2.2. VUV spectroscopy of impurity events

Transient impurity events (TIEs) are also known as unidentified flying objects (UFOs) as they often appear as bright flying objects and are thought to result from small particles or dust contaminating the core plasma. TIEs are characterised by large, often short-lived, spikes in radiated power (Coenen 2013, Sertoli 2014). An example of these impurity driven radiation events is shown in figures 6(*a*)–(*c*). Please refer to the figure caption for more details. These radiation events have a typical rise time of order ms and can, in some cases, lead to a long-lasting growth in radiated power. In severe cases, this can add up to ~1 MW to the steady-state bulk radiated power—a significant contribution. In the most extreme cases, these radiation events can lead to plasma instabilities and even termination of the plasma discharge (an example of the latter is pulse 81781 from figure 5) (Ekedahl 2009, de Vries 2014, Sertoli 2014).

Data from two of JETs VUV survey SPRED spectrometers have been used to investigate the elemental composition of the impurities related to TIEs (Sertoli 2014). These systems monitor the impurity content of the JET plasma across the spectral ranges 100–1000 Å and 140–443 Å, along lines-of-sight at octant 6 (shown in the poloidal cross-section in figure 6(*a*)) (Fonck 1982, Wolf 1995, Coffey 2004). By integrating the VUV signal over known spectral emission lines, events originating from Ni, Fe, Cr, Cu, Al and W impurities can be distinguished. Example data for three sequential TIEs in the same pulse resulting from W impurities is shown in figure 6(*c*).

The occurrence of TIEs has been analysed for JET pulse 80128–85699, which starts with the very first campaign of JET's new ILW (Sertoli 2014). A total of 3388 events have been detected in 4144 plasma discharges (~23 h of plasma), with an average of 1 event every 25 s of plasma. This study shows that the major contributor to TIEs is W, accounting for 51% of all impurity events, with W usually occurring in isolation.

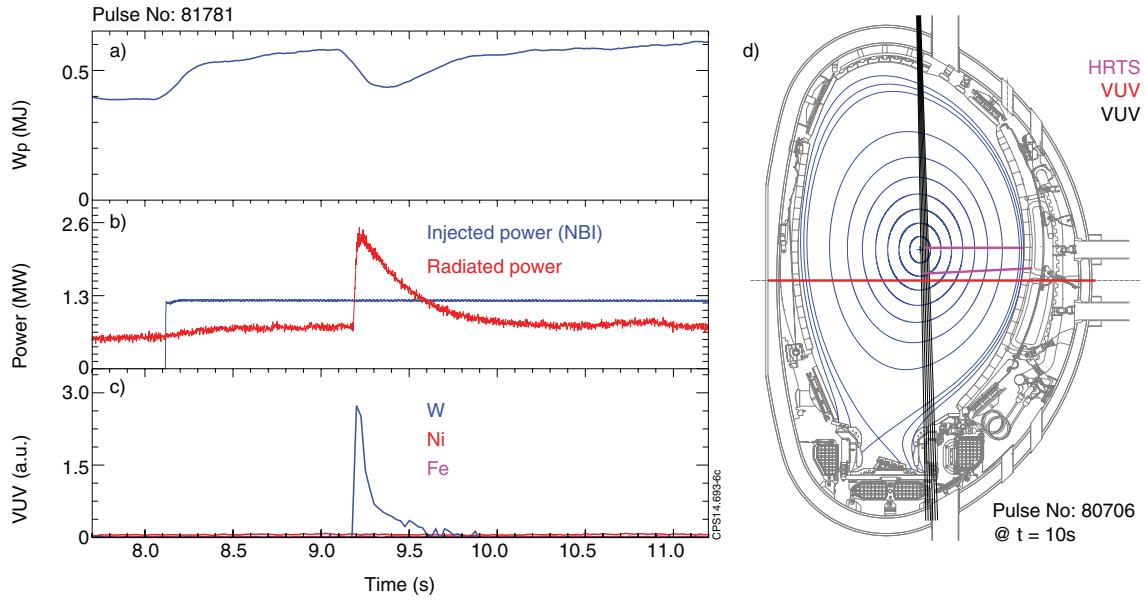

Figure 6. (*a*)–(*c*) Example of a TIE occurring in JET pulse 81781 (*a*) plasma energy W_p, (*b*) power from neutral beam injection (NBI) and radiated power, (*c*) VUV data for W, Ni and Fe lines. (*d*) A cross-sectional view of JET, showing the diagnostic lines-of-sight for HRTS (octant 5) and two VUV diagnostics (both octant 6). Magnetic flux lines for JET pulse 80706 at $t = 10$ s are shown for illustrative purposes.

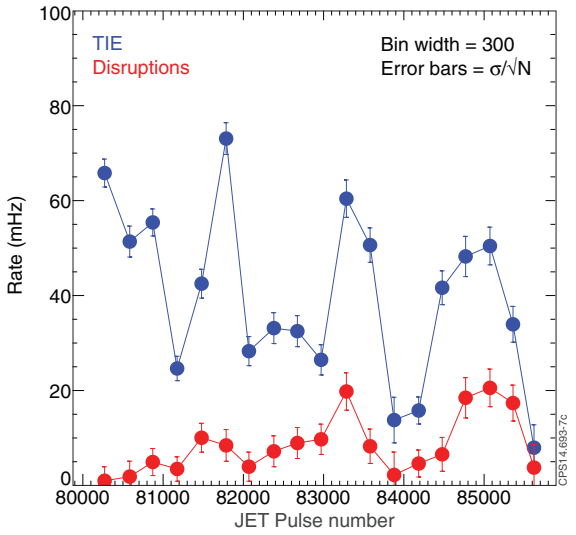

Figure 7. The TIE and disruption rate (normalised to plasma operational time) as a function of JET pulse number (JPN).

26% of all events are correlated with the simultaneous presence of Ni, Fe and Cr, which almost certainly originate from Inconel or steel in-vessel components. The remaining percentage of events corresponds to either Al or Cu, or to events with no clear VUV signature in the spectral range considered (these may result from lighter elements, such as carbon and beryllium). Over the initial ILW operation period, 22 impurity events are induced by material flaking from the reciprocating probe (RCP) diagnostic, used to measure the electron temperature at the upper edge of the JET plasma at octant 5 (Davies 1996). These events are dominated by Ni, Fe and Cr, which is consistent with the material of the probe shaft (Inconel / steel).

A database containing various parameters for every plasma discharge in the TIE analysis pulse range has also been collated in order to explore parametric dependencies (Sertoli 2014). A clear correlation with disruption events is found; TIEs are most likely to occur in the few discharges following a disruption, with the TIE rate 50% higher in the 4 discharges following a disruption. Figure 7 shows the TIE and disruption rate (defined as the number of events per bin, normalised to the total plasma operational time for the discharges in that bin), with a bin width of 300 JET pulses. A strong correlation between the TIE and disruption rate is apparent, with three discreet peaks seen in each data set. The peaks in disruption rate correspond to intentional disruptions associated with experimental sessions studying disruptions, disruption mitigation techniques and runaway electron events. The majority of disruption events in these periods are intentionally induced with typically high displacement forces. The TIE rate follows a very similar trend, with an additional overall downward drift; one that is particularly noticeable for JET pulse < 81200, where the TIE rate decreases by a factor of three in spite of the rise that occurs in the disruption rate over this time. This initial drop is also mirrored in the HRTS dust signal (see section 2.4 for more details). Taken together, these results suggest that an initial inventory of dust, present from the very start of ILW operations, is being gradually removed from circulation. The rises associated with periods of frequent disruptions may indicate that disruptions redistribute dust into more accessible areas. It is not possible to infer from this if disruptions create new dust material. The study in (Sertoli 2014) has also shown that TIEs are far more likely in diverted plasma configurations with the probability of a TIE occurring significantly reduced if the strike point is located on the vertical surface of a divertor tile, as opposed to a horizontal surface. This seems logical, given that dust tends to collect on the horizontal surfaces of the divertor region. Overall, the probability of a severe outcome from a TIE is low; only 25 of the 3388 TIEs studied result in a significant

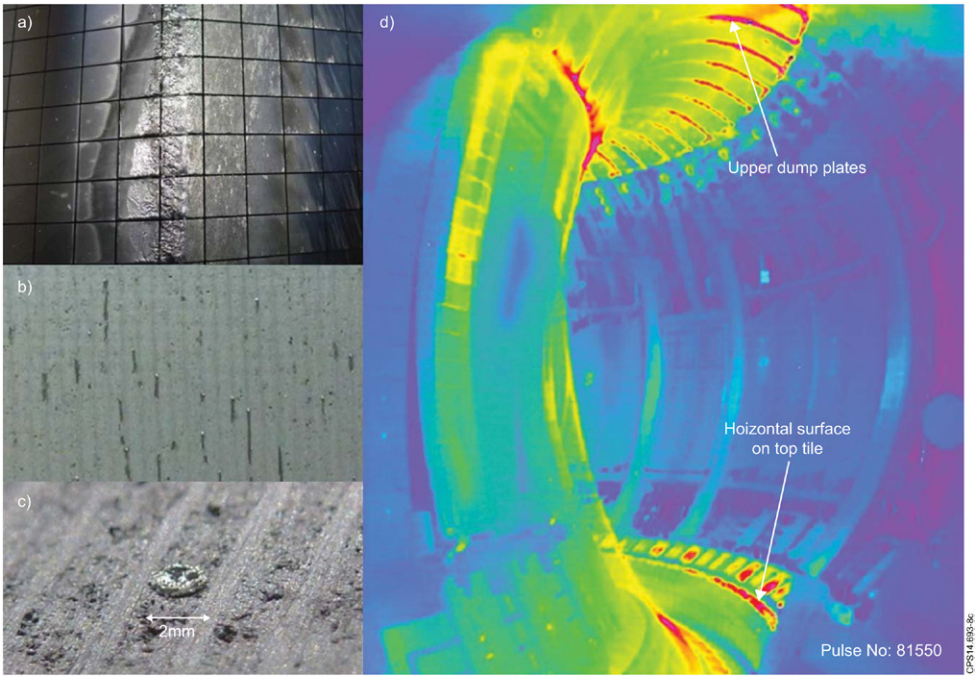

Figure 8. (*a*) Upper dump plate (bulk-Be) showing melting in the centre and the results of arcing on the right hand side (Arnoux 2014). (*b*) and (*c*) show images from the horizontal surface on top tile 8 (W-coated CFC). In (*b*), delamination of the W-coating with small beads of W are visible. (*c*) Shows a small Be droplet. (*d*) Infrared image from the KL7 camera showing the heat loads on the JET ILW during a density limit disruption pulse; JET pulse 81550.

(>60%) drop in plasma energy. And of these, less than 10 result in a disruption in the few seconds after the TIE (cf with ~700 disruptions over the ILW period).

2.3. In-vessel inspection

There are many erosion-deposition diagnostic tools installed into JET's ILW, including beryllium and tungsten marker tiles and wall probes in the main chamber and divertor (Rubel 2013). During a recent intervention period with in-vessel access (just after JET pulse 83934), these diagnostic tools were recovered for analysis. Detailed in-vessel photographic surveys and dust collection was also performed (Widdowson 2014). Here, we present a brief summary of some of the initial dust related findings from these studies. The post-mortem analysis from these studies will continue for some time.

A selection of images from the detailed photographic survey are shown in figures 8(*a*)–(*c*) together with an infrared image from the KL7 camera in (*d*) showing the heat loads on the JET ILW during a density limit disruption pulse (JET pulse 81550). This is shown to illustrate some of the areas of JETs PFCs most at risk. The image in (*a*) shows damage due to melting and arcing on one of the bulk Be upper dump plate tiles. The images in figures 8(*b*) and (*c*) correspond to the upper horizontal surface of the divertor tile 8. In (*b*) delamination of the W coating is seen, with small bead of W visible at the ends of some of the damaged strips. These regions of delamination lie along the CFC fibres and are not seen on all tiles: some are noticeably worse than others. This probably results from the fact that the CFC proved difficult to coat with W (Matthews 2011). In (*c*), a small droplet of Be can be seen, possibly originating from the upper dump plate above.

Dust collection from a portion of the divertor region yielded ~1 g of material; significantly less than the 200 g recovered from the same area during the CW period (Widdowson 2014). Compositional analysis on the dust extracted from the divertor is in progress. Studies of deposition diagnostics reveal that the quantity of deposits in the divertor region is an order of magnitude less than for the CW, with deposits of only a few 100 nm thick observed so far (Widdowson 2014). This reduction in migrated material may be linked to the drop in dust collected to date since there will be a significantly increased time for layers to reach mechanical stability limits. The overall picture from this analysis is that the ILW is a much cleaner environment than the CW, but that mechanisms do exist for the production of metal particulates.

From inspection of the TIE data, we see that there are 1697 events that can be attributed to W across the operational period considered for the ILW. If we assume that the W concentration spikes to approximately 10^{-4} (an upper estimate) in each instance, and assume a volume average electron density of order $10^{20}\,m^{-3}$, we can estimate that there are somewhere in the region of 10^{18} W atoms per TIE (JET plasma volume ~100 m^3). A maximum estimate of the W particle mass required for all observed W TIEs is then ~0.3 g. The 1 g of dust recovered from a portion of divertor thus demonstrates that there is certainly sufficient material (assuming the dust has a representative proportion of W as seen in the TIEs).

However, many parameters influence how impurity particles interact with the plasma (i.e. particle size, injection velocity, plasma parameters) and screening may prevent

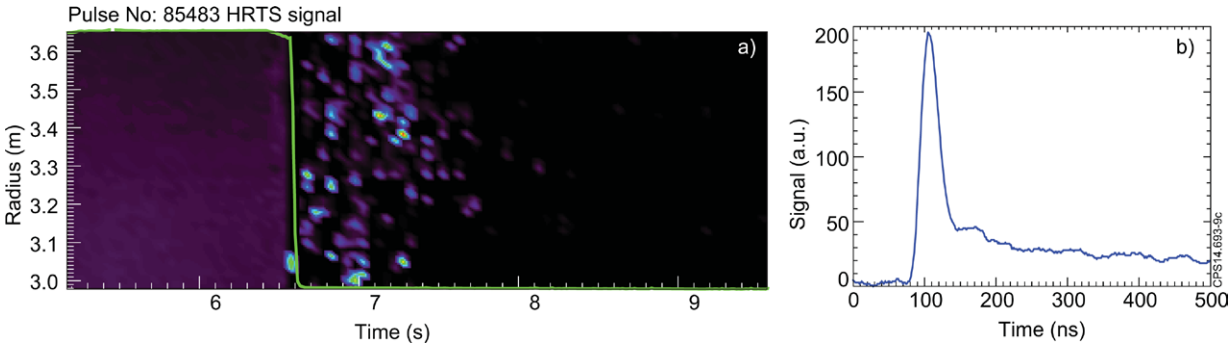

Figure 9. HRTS (*a*) Colour levels show the HRTS signal for JET pulse 85483 as a function of time. The plasma is terminated by a disruption with $t_d = 6.56$ s and $t_m = 6.65$ s. Induced vessel forces are recorded as 0.75 MN. At the time of the disruption, the plasma current (superimposed schematically in green) plummets to zero. At this time, the HRTS signal changes from Thomson scattered light, visible on all spectrometers, to an intermittent dust signal with a characteristic temporal signature, shown in the example in (*b*).

them from entering the core at all. A deeper understanding of this interaction can only be answered with a more sophisticated analysis; such as the numerical modelling described in (Sertoli 2014), which looks at the dust-plasma interaction for the same JET ILW period. In this study, the transport and ablation of tungsten dust particles in the JET plasma has been modelled using the 2D code DTOKS (Bacharis 2010). This work considers W particles injected from the outer strike point with an initial velocity of 10 m s^{-1} (correlating well with observed behaviour, as shown in figure 5). The study considers particle sizes from 10–100 μm and predicts that a maximum of ~50% of a particle's mass is ablated inside the plasma. The 1D STRAHL code has also been used to simulate the impurity transport occurring after the dust ablation from this DTOKS study (Dux 2006, Sertoli 2014). Estimates from this approach indicate that somewhere in the order of 2×10^{17} ions are needed to generate the observed increase in radiated power, which equates to a W particle of ~90 μm in radius. This is a minimum estimate since it does not include screening effects (i.e. ablation with in the scrape-off-layer en route to the plasma core). Allowing for a screening of 50%, this study finds that 0.14 g of W dust would account for the 1697 detected W events; in good agreement with the previous crude estimates. Note also that this estimate of particle size is of the order of the droplets seen during the bulk-W melt experiments (Coenen 2014).

2.4. Laser scattering

JETs high resolution Thomson scattering (HRTS) diagnostic is a conventional Thomson scattering system (Pasqualotto 2004), which has been routinely producing electron density and temperature profiles of the JET plasma since 2007. This system uses a 5 J pulsed Nd:YAG laser fired into the JET vessel through a vacuum window located roughly mid-plane at octant 5 (see figure 6(*d*)). The HRTS diagnostic provides 35 s of data from the start of a JET discharge with a spatial resolution of approx. 1.5 cm. During a plasma discharge, Thomson scattered light from the laser chord is analysed by a bank of spectrometers. In the few seconds immediately following a disruption, large spikes are often seen in the HRTS signal, as shown in figure 9(*a*). These signal spikes originate from the interaction between the laser beam and dust mobilized by the disruption (Giovannozzi 2010). The long decay time of the dust signal detected by the HRTS spectrometers, shown in figure 9(*b*), is typical of light emitted from a source that has been heated or ablated by a laser pulse. Typically, dust signals are detected for a period of approx. 1–3 s following a disruption.

The HRTS system thus provides an automatic measure of the quantity of dust mobilized by a disruption event. However, limitations of this technique should be appreciated; the volume of the JET vessel sampled by the HRTS laser chord is small and signal is only detected when dust crosses the chord. Cases are noted where dust / debris visible on JETs camera systems does not intersect the HRTS chord (an example was shown in figure 3). In addition, it is not simple to infer particle size from the event magnitude, since different materials are expected to have different intrinsic brightness when interacting with the pulsed laser. Surface quality and any surface coatings present may also play a role in determining the brightness of any given dust-laser interaction event. Furthermore, it is not possible to distinguish between many particles in close proximity and a single large event, and a particle moving along the laser chord will be recorded as multiple events. When added to the fact that this measure of the dust inventory is only made infrequently (i.e. with disruptions), one must be cautious about interpreting the resulting data. However, by analysing the HRTS signal across many disruption events, we find that it is possible to extract trends and explore relationships.

The parameters that are extracted from the HRTS dust signal for analysis are:

(a) The total signal (T_{sig}): this is the integrated signal level of all dust events detected in a single disruption; i.e. the total 'brightness'.
(b) The total number of events (N_{dust}): this is the total number of signal spikes detected in a single disruption; i.e. the number of dust particles (to first order approximation).

These parameters can be generated automatically using a variant of the code used to provide the electron temperature and density data from this diagnostic. HRTS dust data is available for 363 disruptions in the very latter part of the CW period (for JET pulse 73337–79853) and for 695 disruptions

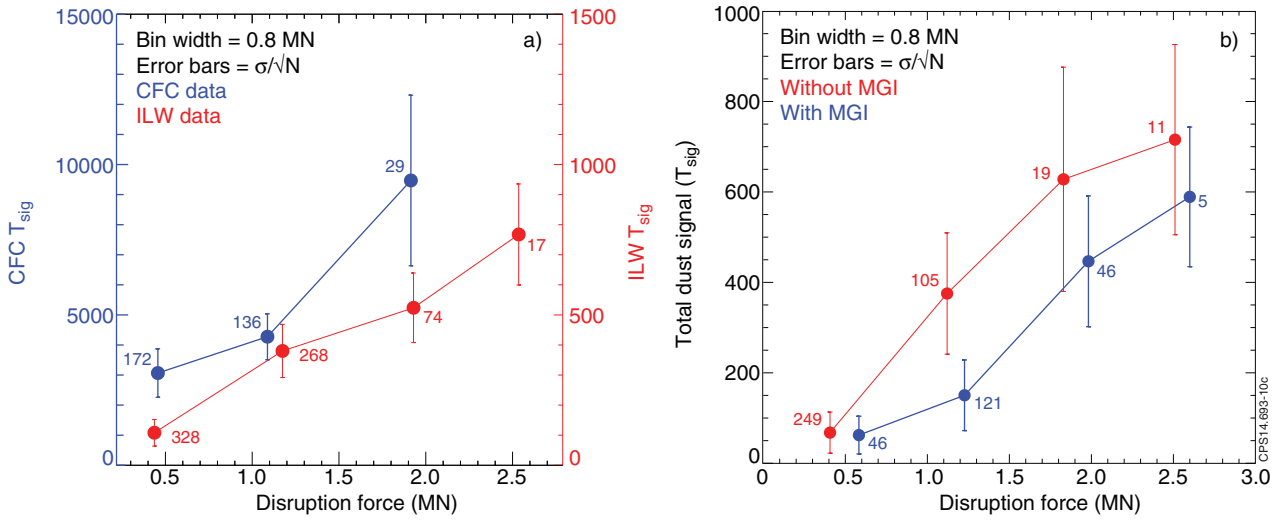

Figure 10. (*a*) HRTS total dust signal T_{sig} for both the CW (blue) and ILW (red) as a function of disruption force. Note that the CW data is plotted on a vertical scale 10 times larger than for the ILW data. Each data point corresponds to the average value in a bin of width 0.8 MN with error bars of $\sigma/\sqrt{N}$, where N is the number of disruption events in that bin and σ is their standard deviation. The value of N is shown on the figure, next to the corresponding data point. (*b*) A similar plot as (*a*), but for ILW data only, for disruptions with (blue) and without (red) use of disruption mitigation via massive gas injection (MGI). Data in (*b*) only includes pulses for which the disruption mitigation system was fully active: JET pulse 81560–85977.

in the period of operation to date with the ILW (for JET pulse 80128–85978). The most striking result from this analysis is that the amount of dust seen is significantly smaller for the ILW than for the CW period, by a factor of 20 (on average) for the total dust signal and a factor of 30 (on average) for the number of dust events. This is in rough agreement with the differences in the mass of dust collected from the vessel during CW and ILW intervention periods (see section 2.3 for more detail).

Further analysis shows that there is a clear positive correlation between the disruption force and the HRTS dust parameters, as shown in figure 10(*a*) which shows T_{sig} for both the CW (blue) and ILW (red) as a function of disruption force. Please see the figure caption for further details. A very similar relationship is seen for N_{dust} (not shown here for brevity). This relationship confirms a somewhat intuitive expectation; that the amount of dust shaken free is proportional to the vessel displacement forces. However, as for the case of the TIE analysis, this provides no information on what fraction of dust might be created by a disruption as opposed to merely mobilized.

Information on the effect of disruption mitigation via massive gas injection (MGI), known to reduce forces and heat loads, can also be gained from the HRTS dust data. In figure 10(*b*), the ILW T_{sig} data from (*a*) is re-plotted, with all events split into two data sets: accounting for whether or not MGI was used to mitigate the disruptions. Both data sets show the same increasing trend with disruption force, with a difference in magnitude. The amount of data here is somewhat limited, with error bars producing overlapping data sets for much of the force range. However, for the second force bin, located at ~1.25 MN, it can be seen that there is a clear drop with the average T_{sig} reduced by a factor of 1.6 (on average) in the case of MGI (N_{dust} is similarly reduced, by a factor of 1.9). Note that this observed reduction in dust is for disruptions of the *same* force. When the force reduction of the MGI is taken into account, this demonstrates that the use of MGI can reduce the dust mobilized by a disruption by approximately a factor of 4.

The evolution of the HRTS dust signals over the first five campaigns of the ILW period (covering JET pulse 80128–85977) is shown in figure 11. Light blue and red points with vertical markers show data for individual disruptions. Dark blue and red points show average values for a bin width of 300 pulses. The individual disruptions with values far higher than the global average are explained in figure 12(*a*) and surrounding text. In the initial period (up to JET pulse 81400), there is a rapid decline, with the drop in N_{dust} closely mirroring the fall in the rate of TIEs seen over this period. As previously mentioned, this suggests that material present prior to the start of the ILW plasma operations has been gradually removed from circulation. Small particles of debris visible on images of divertor tiles taken before ILW operations began add weight to this theory. Images of the same tiles taken just after JET pulse 82929, when both the TIE and HRTS signal levels are significantly reduced, are clear of debris. Inset, in Figures 11(*b*) and 12, the evolution of T_{sig} past the initial period of steep decline is shown (for JET pulse > 81400). Here, several peaks in T_{sig} can be seen, superimposed on an overall downward trend, which match the fluctuations in the TIE rate over the same period (plotted in blue). This correlation adds further weight to the theory that TIEs are caused by dust particles.

While T_{sig} and N_{dust} show a strong correlation (on average) and both display similar trends with disruption force, their ratio shows a large degree of variation. In an attempt to further understand this, we find it useful to plot T_{sig} as a function of N_{dust} for each disruption, as shown in figure 12. Displaying the data in this way allows the most extreme events to be clearly

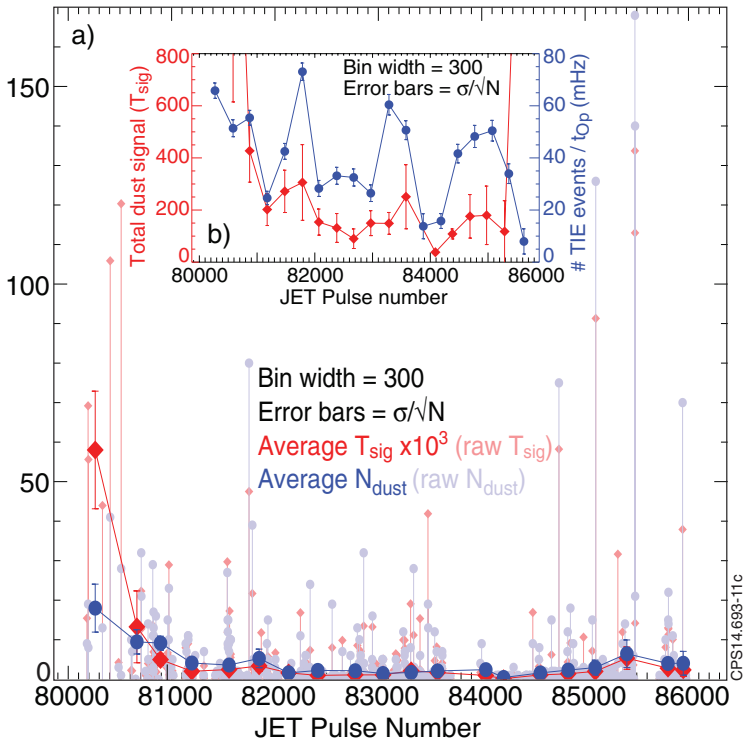

Figure 11. (*a*) HRTS T_{sig} (diamonds) and N_{dust} (circles) as a function of JET pulse number (JPN) 80128–85977, corresponding to the first 5 campaigns of the ILW period. Light blue and red points with vertical markers show raw data for individual disruptions. Dark blue and red points show average values over 300 pulses. Error bars are defined in the caption to figure 10. (*b*) inset, shows T_{sig} on a smaller scale, together with TIE rate data from figure 7.

identified. By exploring the details of these events, we see patterns emerge; the events in figure 12 with high values of both T_{sig} and N_{dust} (circled) correspond to discharges in which the reciprocating probe (RCP) diagnostic was malfunctioning, introducing material into the vessel. As mentioned in section 2.2, VUV analysis has shown that impurities associated with these events are consistent with the materials of the probe shaft (Sertoli 2014).

The disruptions with very high values of T_{sig} but lower values of N_{dust}, are all found to lie in the very early part of the ILW operational period—within the first 10 disruptions. On closer inspection of the HRTS data we see that, in each case, the very high signal level can often be attributed in the major part to just a few dust events. This suggests that the high values of T_{sig} after disruptions at this time period may have resulted from a few large dust particles that were later fragmented / eroded. Other high magnitude events are also found to be associated with an influx of material, within that same pulse, from a range of sources. These are indicated in the legend on figure 12(*a*) and include tungsten influx from the divertor region (as shown in figure 5), beryllium droplets from melt damage (as described in figures 4 and 8(*a*) and surrounding text), in addition to copper influx (possibly from the neutral beam injection system).

3. Discussion and conclusions

The results presented here have shown that the amount of dust for the ILW is low and, at present, is decreasing with operational time. These results also suggest that disruptions primarily act to mobilize the existing quota of dust, moving a subset of this material into areas more accessible to the plasma. These re-positioned dust particles are then more likely to appear as transient impurity events (TIEs) in subsequent plasma discharges, where they are partially consumed and later re-deposited as thin films onto the plasma facing components. It should be noted that the methods used here are very poor indicators of how much of the dust seen after a disruption might be created in that event, as opposed to merely mobilized. The fact that dust levels are decreasing with time despite relative frequent disruptions (many of them deliberately induced for studies of disruption physics etc) suggests that little, if any, dust is created during a disruption. However, for moderate disruption forces, the amount of dust seen for mitigated disruptions is notably reduced. Since mitigated disruptions lower heat loads to the plasma facing components, this may indicate that unmitigated disruptions do indeed create some material.

The high TIE rate and (relatively) large amounts of dust seen after disruptions during the early period of operation with the ILW points to material left in the vessel after the installation of the ILW was completed. Over time, these particles appear to have been gradually removed from circulation (via processes of erosion / fragmentation and possible re-positioning into in-accessible areas, such as the spaces behind the first wall tiles). Some events during plasma operations have also been seen to add to the quota of particulate matter, but, at present, the rate at which this material is removed from

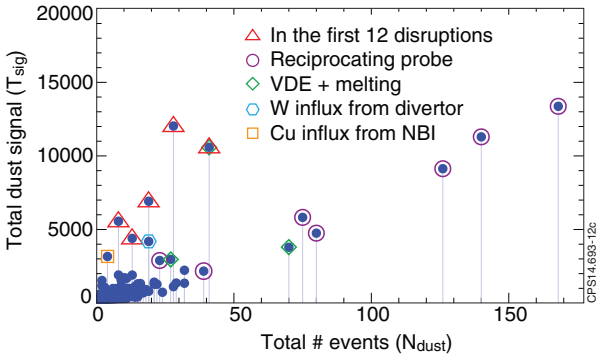

Figure 12. HRTS dust data: Total signal versus total number of events. Each data point represents a single disruption event. Additional details for extreme events are noted in the legend.

circulation is greater than any accumulation. As re-deposited layers build up and reach mechanical stability limits, this may change. However, the rates of material migration are orders of magnitude lower than for the carbon-wall and this may not happen for some time.

The effect of dust particles on plasma operations seems to be tolerable, with large losses to plasma energy or confinement relative rare. However, a few (of the handful) of impurity induced disruptions account for some of the most extreme disruptions in the ILW history to date; the highest disruption forces for an unintentional disruption, of 3.21 MN, occurred after a large W-influx from the divertor region. However, it should be noted that in this case, the disruption was unmitigated. The, now more routine, use of a massive gas injection in response to disruption precursors will obviously lessen the impact of such events.

Numerical modelling of the transport and ablation of W dust particles in the JET plasma confirm that W particles of a feasible size are capable of generating radiation events of the magnitude seen in JET plasmas (Sertoli 2014). This modelling work also helps to confirm that there is sufficient material generated from the (relatively small amounts) of damage seen to the tungsten parts of the plasma facing components to account for the number of TIEs seen during the operation period of the ILW to date. Further studies of particle influx in images from JET camera systems and analysis of the collected dust in terms of size and composition should allow for further refinement of input parameters to these models.

In conclusion, although impurities from in-vessel dust can, in extreme cases, have undesirable effects on plasma performance, taken together, the results shown here are encouraging for future devices such as ITER. The recent operational period of JET with the ILW has demonstrated that despite an initial inventory of material, and with repeated additions to this inventory, there exist efficient mechanisms that act to remove dust from circulation during normal plasma operations. Whether these mechanisms will succeed in balancing dust production as JET continues operations or in larger devices is, of course, another question and one that requires significantly more study to understand. However, since dust particle sizes are unlikely to scale with the vessel dimensions, the relative impact of individual impurities events should reduce for larger devices, such as ITER.

Acknowledgments

This work was supported by EURATOM and carried out within the framework of the European Fusion Development Agreement and the RCUK Energy Programme [grant number EP/I501045]. The views and opinions expressed herein do not necessarily reflect those of the European Commission or ITER.

References

Arnoux G 2010 Heat load measurements on the JET first wall during disruptions *Proc. 19th Int. Conf. on Plasma Surface Interactions* (*San Diego, CA*)

Arnoux G 2014 Power handling of the JET ITER-like wall *Phys. Scr.* **2014** 014009

Bacharis M 2010 Dust in tokamaks: an overview of the physical model of the dust in tokamaks code *Phys. Plasmas* **17** 042505

Bell A 2002 Tritium inventory control—the experience with DT tokamaks and its relevance for future machines *Proc. SOFT 2002* (*Helsinki, Finland*) p 913

Clever M 2013 A wide angle view imaging diagnostic with all reflective, in-vessel optics at JET *Fusion Eng. Des.* **88** 1342–6

Coenen J 2013 Long-term evolution of the impurity composition and impurity events with the ITER-like wall at JET *Nucl. Fusion* **53** 073043

Coenen J 2014 ELM induced tungsten melting and its impact on tokamak operation *Proc. 21st Int. Conf. on Plasma Surface Interactions (PSI)* (*Kanazawa, Japan*)

Coffey I 2004 First tritium operation of ITER-prototype VUV spectroscopy on JET *Rev. Sci. Instrum.* **75** 3737

Craciunescu T 2014a An original method for spot detection and analysis for large surveys of videos in JET *IEEE Trans. Plasma Sci.* **42** 1358–66

Craciunescu T 2014b Overview of image processing tools to extract physical information from JET videos *Proc. 8th Workshop on Fusion Data Processing, Validation and Analysis* (*4–6 November 2013*)

Davies S 1996 The JET reciprocating probe systems—performance and data analysis *Contrib. Plasma Phys.* **36** 117–23

de Vries P C 2014 The influence of an ITER-like wall on disruptions at JET *Phys. Plasmas* **21** 056101

Dux R 2006 STRAHL User Manual, IPP Garching: Laborberiicht 10/30

Ekedahl A 2009 Analysis of radiative disruptions in RF-heated Tore Supra plasmas using infrared imaging *J. Nucl. Mater.* **390–391** 806–9

Fonck R 1982 Multichannel grazing incidence spectrometer for plasma impurity diagnosis: SPRED *Appl. Opt.* **21** 2115

Giovannozzi E 2010 Detection of dust on JET with the high resolution Thomson scattering system *Rev. Sci. Instrum.* **81** 10E131

Huber A 2012 Development of a mirror-based endoscope for divertor spectroscopy on JET with the new ITER-like wall *Rev Sci. Instrum.* **83** 10D511

Krasheninnikov S I 2011 Dust in magnetic fusion devices *Plasma Phys. Control. Fusion* **53** 083001

Lehnen M 2010 Disruption mitigation by massive gas injection in JET *Proc. 23rd IAEA Fusion Energy Conf.* (*Daejon, Republic of Korea*)

Lescure C 2009 Measurement of disruption forces in JET using fiber-optic sensors *Proc. 36th Int. Conf. on Plasma Science and 23rd Symp. on Fusion Engineering Conf. ICOPS-SOFE 2009 (San Diego, CA, 31 May 2009–5 June 2009)*
Marchese V 1996 Enhancement of JET machine instrumentation and coil protection *Proc. 19th SOFT 1996 (Lisbon, Portugal)* p 747
Matthews G F 2011 JET ITER-like wall—overview and experimental programme *Phys. Scr.* **2011** 014001
Pasqualotto R 2004 High resolution Thomson scattering for Joint European Torus (JET) *Rev. Sci. Instrum.* **75** 3891
Ratynskaia S 2011 Diagnostics of mobile dust in scrape-off layer plasmas *Plasma Phys. Control. Fusion* **53** 074009
Rosanvallon S 2009 Dust limit management strategy in tokamaks *J. Nucl. Mater.* **390–391** 57–60
Roth J 2009 Recent analysis of key plasma wall interactions issues for ITER *J. Nucl. Mater.* **390–391** 1–9
Rubel M 2013 Overview of erosion-deposition diagnostic tools for the ITER-like wall in the JET tokamak *J. Nucl. Mater.* **438** S1204–7
Sertoli M 2014 *Impact of W Events and Dust on JET-ILW Operation* (Japan: Ongaku-do, Kanazawa Ishikawa)
Widdowson A 2014 Material migration patterns and overview of first surface analysis of the JET ITER-like wall *Proc. 14th Int. Conf. of Plasma-Facing Materials and Components for Fusion Applications* (*Julich, Germany*)
Wolf R 1995 A vacuum ultra-violet spectrometer (Double_SPRED) for the observations of the JET divertor plasma *Rev. Sci. Instrum.* submitted